

Geometrical Characterization of Glass Nanopipettes with Sub-10 nm Pore Diameter by Transmission Electron Microscopy

Kazuki Shigyou,¹ Linhao Sun,¹ Riku Yajima,² Shohei Takigaura,³ Masashi Tajima,⁴ Hirotohi Furusho,¹ Yousuke Kikuchi,⁵ Keisuke Miyazawa,^{6,1} Takeshi Fukuma,^{1,7} Azuma Taoka,^{5,1} Toshio Ando,^{1,*} and Shinji Watanabe^{1,†}

¹*Nano Life Science Institute (WPI-NanoLSI), Kanazawa University, Kakuma-machi, Kanazawa 920-1192, Japan[‡]*

²*Division of Nano Life Science, Graduate School of Frontier Science Initiative, Kanazawa University, Kakuma-machi, Kanazawa 920-1192, Japan*

³*Department of Physics, Institute of Science and Engineering, Kanazawa University, Kakuma-machi, Kanazawa 920-1192, Japan*

⁴*College of Science and Engineering, Kanazawa University, Kakuma-machi, Kanazawa 920-1192, Japan*

⁵*Institute of Science and Engineering, Kanazawa university, Kakuma-machi, Kanazawa 920-1192, Japan*

⁶*Faculty of Frontier Engineering, Institute of Science and Engineering, Kanazawa University*

⁷*Faculty of Frontier Engineering, Institute of Science and Engineering, Kanazawa University, Kakuma-machi, Kanazawa 920-1192, Japan*

Glass nanopipettes are widely used for various applications in nanosciences. In most of the applications, it is important to characterize their geometrical parameters, such as the aperture size and the inner cone angle at the tip region. For nanopipettes with sub-10 nm aperture and thin wall thickness, transmission electron microscopy (TEM) must be most instrumental in their precise geometrical measurement. However, this measurement has remained a challenge because heat generated by electron beam irradiation would largely deform sub-10-nm nanopipettes. Here we provide methods for preparing TEM specimens that do not cause deformation of such tiny nanopipettes.

INTRODUCTION

Glass nanopipettes have numerous applications in nanosciences, such as single molecule sensing of macromolecules and their interactions [1] and local delivery of molecules [2]. In many applications (if not all), the nanopipette geometrical parameters, such as the inner and outer cone angles, pore and central channel diameters, and wall thickness are important determinants of the application performance [3], as typically seen in scanning ion conductance microscopy (SICM) [4–7]. The spatial resolution of SICM is strongly dependent on the nanopipette tip geometry [8–13]. The assessment of detailed tip geometry is thus important for the optimization of nanopipette-based measurements. Two methods and their combination have been widely used for this assessment: electrical measurements of the ion current resistance and scanning electron microscopy (SEM) imaging [12]. The ion current resistance is related to the pore diameter and the inner half cone (IHC) angle [14–16]. The IHC angle cannot be directly assessed in both measurements. Therefore, it is usually estimated from the outer cone angle given by SEM images of the nanopipette by assuming a constant ratio of outer to inner radius, or from the pore size given by SEM images and the ion current resistance [12]. When nanopipette fabrication can be performed with good reproducibility of a constant geometry, the pore diameter can be estimated from the electrical measurement alone using the IHC angle pre-estimated from SEM measurements for a few nanopipettes. However, SEM visualizes the pipette outer shape and pore after pretreatment with metal-coating,

and therefore, the measured geometrical parameters are affected by the metal-coating.

Direct observation of the detailed tip geometry of nanopipettes has been achieved using transmission electron microscopy (TEM) [15, 17, 18]. From their TEM images, the pore diameter, IHC angle, and the internal channel can be directly and accurately measured. However, it is still challenging to perform TEM measurements for pipettes with pore diameter less than 30 nm [15], particularly to get their consistent images. In TEM measurements of smaller nanopipettes with thin wall, deformation of their tip caused by the electron beam-generating heat is a serious problem [17]. The optimization of TEM measurements is therefore important in overcoming this heating problem and thereby achieving precise characterization of the geometry, particularly for nanopipettes with sub-10 nm diameter (referred to as sub-10-nm nanopipettes hereafter).

In this report, we describe methods to fabricate sub-10 nm nanopipettes with good reproducibility and to characterize their tip geometry with TEM without causing tip deformation. In addition, we provide an easy method to prepare a large number of tip segments on a TEM grid. These methods facilitate tuning and optimization of sub-10 nm nanopipette fabrication for practical applications.

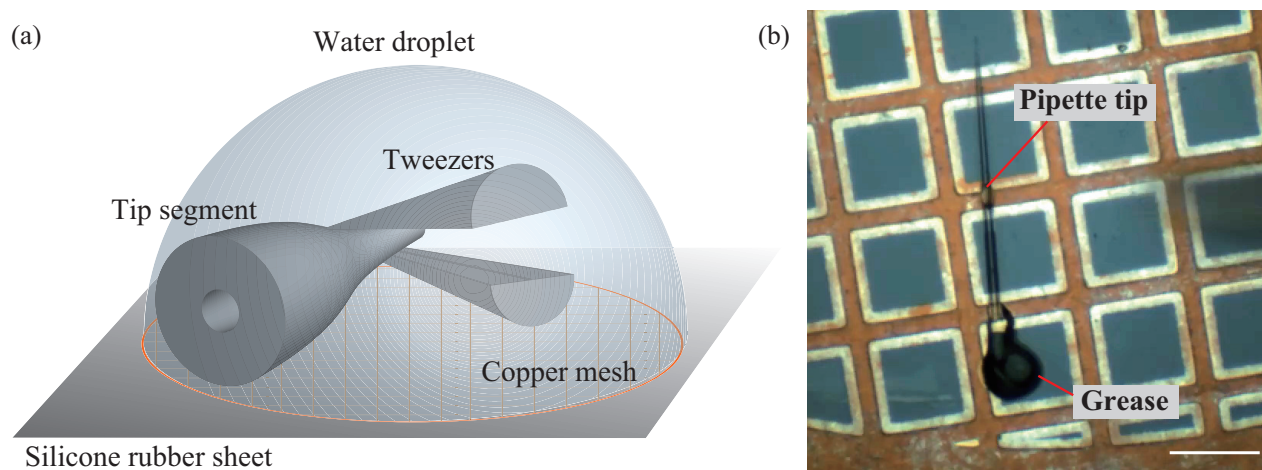


Figure 1. (a) Schematic for cutting of a nanopipette to produce a tip segment in a water droplet on TEM grid. (b) Optical microscope image showing a tip segment appropriately positioned and glued on the TEM grid. Scale bar, 100 μm .

MATERIALS AND METHODS

Materials.

2 M KCl and 50 mM FeCl_3 solutions were prepared using deionized (DI) Milli-Q water (resistivity, $\sim 18 \text{ M}\Omega \cdot \text{cm}$ at 25°C). The FeCl_3 solution was used to prepare Ag/AgCl electrodes [19]. KCl and FeCl_3 were purchased from Funakoshi Co. (Tokyo, Japan) and Sigma-Aldrich (MS, USA), respectively. A flexible syringe needle made of plastic and fused silica (World Precision Instruments, Microfil, MF34G-5) was used to fill nanopipettes with DI water or KCl solution.

Sub-10 nm Nanopipette Fabrication.

All sub-10 nm nanopipettes used in this study were fabricated from quartz capillaries with an inner diameter of 0.3 mm and an outer diameter of 1.0 mm (Q100-30-1.5, Sutter Instrument, CA, USA). The capillaries were cut into 75 mm length with a custom-made pipe cutter. Nanopipettes were then fabricated with a laser puller (P-2000, Sutter Instrument, CA, USA). The details of pulling parameters used for the laser puller are provided in Supporting Information, Table S1.

Current-Voltage Curve Analysis.

The current-voltage ($I-V$) relationship was measured using the method previously described [20] to estimate the nanopipette pore diameter before TEM measurements. The nanopipettes were first filled with DI water by a thermally driven method [20]. Then, a large fraction ($>98\%$) of water inside the pipette was replaced with

2 M KCl solution by injecting it. The nanopipettes were incubated for 10 min. For assurance of full solution exchange, the nanopipettes were subsequently immersed in a bath solution of 2 M KCl for 10 min. The absence of a concentration gradient in the tip was confirmed by an $I-V$ measurement over time (Supporting Information, SI 8).

Before the measurement, the tip of the pipette was washed with DI water to remove any contamination. Ag/AgCl electrodes were prepared by dipping Ag wires into 50 mM FeCl_3 solution for one min [19]. The ion current was amplified with an amplifier (Axopatch 200B, Molecular Devices, LLC, CA, USA). A Faraday cage was used to suppress electrical noise in the $I-V$ measurements. A narrow range of bias voltage (between -40 to $+40$ mV) was used, in which ion current rectification was negligible (Figure. S6). The pipette resistance (V/I) was analyzed as a function of measured pore diameter, IHC angle, and ion conductivity (21.62 S/m at 25°C for 2 M KCl) using a lab-made program based on MATLAB (MathWorks, Inc., MA, USA).

Sample Rreparation for TEM Observations.

After the $I-V$ measurements, the 2 M KCl solution in the nanopipettes was exchanged to DI water. These pipettes were then stored overnight in DI water to remove residual ions. To have a short segment containing the intact tip portion of a nanopipette, the nanopipette was cut in a 12 μL deionized water droplet on a TEM grid, using a micromanipulator and a micro-tweezers (AxisProSS, Micro Support, Shizuoka, Japan) (Supporting Information, Movie 1). The water droplet functions as (i) a cushion against damage of the tip end that would otherwise occur when a cut segment is deposited on the TEM grid, and as (ii) a cage that traps the cut segment in the water

droplet. The TEM grid was placed on a hydrophobic silicone rubber sheet (Figure 1a), which facilitated the formation of a hemisphere-shaped water droplet on the TEM grid. After cutting a number of nanopipettes in this way, we confirmed that all the resulting segments were on the TEM grid. After full evaporation of the water droplet, the tip segments were properly positioned on the TEM grid, using the micromanipulator with a probe (Supporting Information, [Movie 2](#)). TEM copper grids with or without a formvar/carbon membrane were used to investigate how the membrane affects the heat-induced tip deformation during TEM measurements.

TEM Measurements.

The TEM grid on which the nanopipette segments had been properly positioned was placed in the chamber of the TEM apparatus (JEOL 2100 plus). TEM measurements were performed at 200 kV acceleration voltage. The minimum dose system (MDS), a measurement mode in the TEM apparatus, was used to minimize tip deformation. In the MDS, the electron beam irradiates the sample only when the TEM image is captured. The beam irradiation time for capturing an image was set at one second. By utilizing the MDS, we were able to precisely control the total amount of electron dose during imaging, which allowed us to examine an effect of heat generated by electron-beam irradiation. All TEM images were captured at a magnification range between $\times 40,000$ and $\times 80,000$. The electron dose during image acquisition was estimated from the current density.

RESULTS AND DISCUSSION

Fabrication of Nanopipettes.

Sub-10 nm nanopipettes were fabricated using the laser puller P-2000, in which a 75 mm long glass capillary was clamped at their ends. The parameters for the puller action listed in Supporting Information, [Table S1](#), were used. We noticed that the precise control of heat dissipation during the pulling process was important for producing sub-10 nm pipettes with high reproducibility. The rate and amount of heat dissipation are sensitive not only to the area and position at which the glass capillary is clamped but also to the clamping force. The silicone rubber used to clamp a glass capillary deforms depending on the magnitude of clamping force. Therefore, the shape of a produced nanopipette is affected by the clamping force. To control the clamping force precisely, we used a torque driver and a custom screw head. Details are provided in Supporting Information, [Section SI 2](#).

Alignment of Nanopipette Segments on TEM Grid.

Figure 1 shows how a short tip segment was prepared on a copper mesh TEM grid. Using a micro tweezers, a nanopipette whose back side was held was cut in a water droplet on the TEM grid supported on a silicone rubber sheet (Figure 1a). The water droplet prevented the resulting tip segment from escaping from the TEM grid and also from damage, allowing us to efficiently prepare a large number of segments on a TEM grid (Supporting Information, [Movie 1](#)). After the water droplet evaporated, the segments remained on the grid but their position and orientation unavoidably changed; their tip portions were often superposed on the copper mesh. We used the micromanipulator with a glass probe to move each segment so that its tip end portion was not superposed on the copper mesh. Before the positional adjustment of a segment, it was necessary to put a small amount of silicone grease on the back end of the segment. The segment would otherwise be knocked off the TEM grid because of electrostatic interactions between the segment and the glass probe. Figure 1b shows a magnified image of a tip segment on a TEM grid after its positional adjustment. The entire process of this positional adjustment is provided in Supporting Information, [Movie 2](#) and [Section SI 3](#).

Importance of Membrane on TEM Grid.

Here we describe the importance of the use of a formvar/carbon-coated grid in TEM measurements of the sub-10 nm nanopipette tip. The tip portion of a sub-10 nm nanopipette segment must be more susceptible to electron beam-generating heat, compared to a tip with a larger pore and a thicker wall. In TEM measurements, the use of a membrane-coated TEM grid is known quantitatively to suppress heat damage of specimens. However, the effectiveness of the suppression largely depends on the specimen used. We investigated how the tip segment of a sub-10-nm nanopipette would deform during its TEM measurements using TEM grids with and without a formvar/carbon membrane.

Figure 2 shows time-lapse TEM images of tip segments placed on TEM grids with and without the membrane. These segments were obtained from two nanopipettes fabricated under an identical condition. These TEM images were captured at 1 frame/s with an electron dose rate (EDR) of $25.7 \text{ e}^- \text{ \AA}^{-2} \text{ s}^{-1}$. The TEM images taken without the membrane (Figure 2c–e) show noticeable deformation at the tip region even at $t = 1 \text{ s}$. This deformation becomes significant at $t = 2$ and 3 s . In contrast, the TEM images taken with the membrane (Figure 2f–h) show no discernible deformation even at $t = 30 \text{ s}$. Note that the pore diameter of nanopipettes subjected to the TEM observations are expected to be

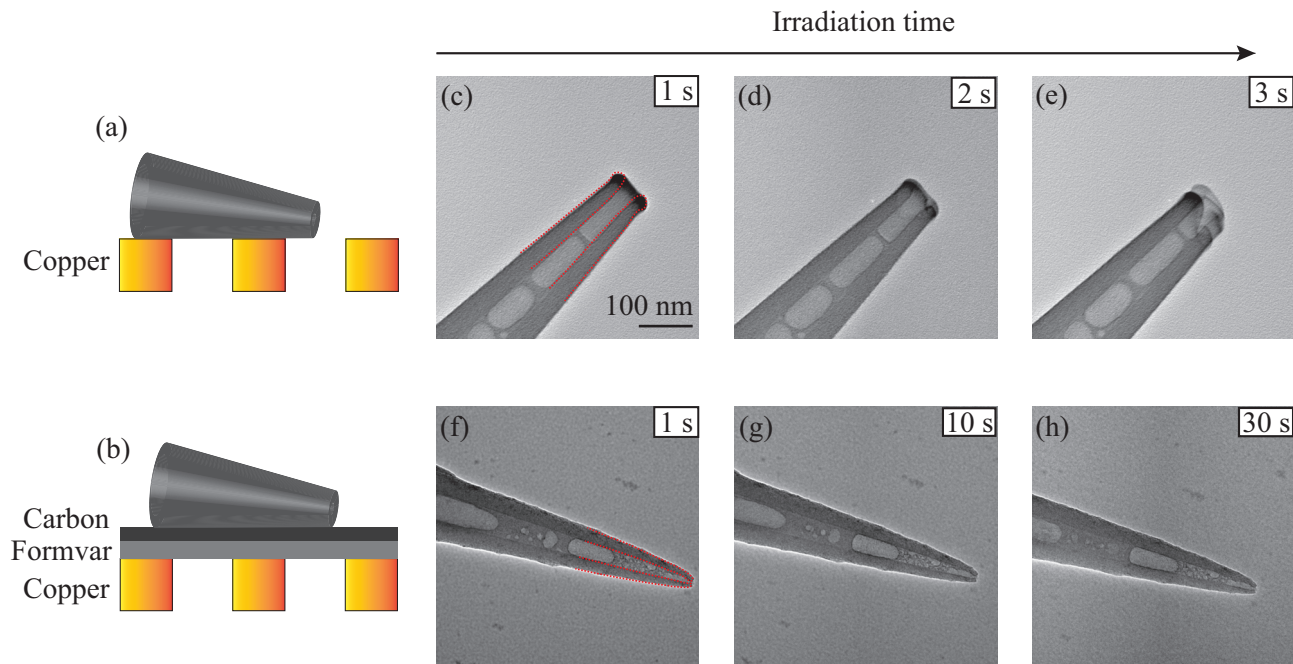


Figure 2. (a, b) Schematics of nanopipette tip segments on copper mesh TEM grids without (a) and with the formvar/carbon membrane (b). (c–h) Time-lapse TEM images of sub-10 nm nanopipettes on the membrane-less TEM grid at 1 to 3 s (c–e), and of those on membrane-coated TEM grid at 1 to 30 s (f–h). The broken red lines are a visual guide to the pipette wall outlines. Note that nano-bubble-like structures are seen in the TEM images (see Supporting Information, Section SI 5 and Movie 3).

within $7.1 \text{ nm} \pm 1.1 \text{ nm}$ (SD, $n = 8$, as described later) before the TEM measurements. We had confirmed this original identical size by measuring ion conductance of these two nanopipettes before their TEM observations. Therefore, the tip shape had already been deformed into a trumpet-like shape at $t = 1 \text{ s}$, when the membrane-less TEM grid was used. In fact, when a membrane-less TEM grid was used, we always observed the trumpet-like shape, even under electron irradiation with a lower EDR of $2.3 \text{ e}^- \text{ \AA}^{-2} \text{ s}^{-1}$ (Supporting Information, Section SI 4, Figure S3). In contrast, when a membrane-coated TEM grid was used, a semi-conical tip shape was always observed.

We further evaluated the heat-induced deformation and the membrane effect against this deformation by varying the irradiation electron density in the TEM measurements (Figure 3). In this evaluation, the outer diameter of the tip end was measured as a function of ED. The EDR was changed in a stepwise manner from 2.3 to $167.5 \text{ e}^- \text{ \AA}^{-2} \text{ s}^{-1}$. When a membrane-less TEM grid was used, the tip outer diameter increased even under the condition of $\text{EDR} = 2.3 \text{ e}^- \text{ \AA}^{-2} \text{ s}^{-1}$, from 35.5 nm (Figure 3b) to 44.4 nm during the period from $t = 2 \text{ s}$ to 5 s (the first two blue circles in Figure 3b). This large increase was followed by a gradual increase up to 60 nm at $t = 30 \text{ s}$ (the next five blue circles in Figure 3a). When the EDR was increased from 2.3 to $23.5 \text{ e}^- \text{ \AA}^{-2} \text{ s}^{-1}$, the tip outer diameter suddenly increased from 60 to 70 nm at $t = 31 \text{ s}$

(Figure 3c). In contrast, when a membrane-coated TEM grid was used, there was no discernible deformation of the tip even at $\text{EDR} = 167.5 \text{ e}^- \text{ \AA}^{-2} \text{ s}^{-1}$, the maximum EDR value for our TEM system (Figure 3d–g). The tip outer diameter remained $\sim 18.5 \text{ nm}$ throughout the observations (red circles in Figure 3a; $18.65 \pm 0.73 \text{ nm}$ (SD), $18.62 \text{ nm} \pm 0.65 \text{ nm}$ (SD), 18.61 ± 0.19 (SD) nm, and $18.10 \text{ nm} \pm 0.65 \text{ nm}$ (SD) for 2.3 , 23.5 , 87.6 , and $167.5 \text{ e}^- \text{ \AA}^{-2} \text{ s}^{-1}$, from left to right), indicating effective dissipation of electron beam-generating heat through the membrane. We confirmed this absence of deformation for 26 sub-10 nm nanopipette tips (not shown). In Supporting Information, Table S2, we provided statistics for tip geometry of eight nanopipettes fabricated using the same pulling parameters, as shown in Supporting Information, Table S1. The tip outer diameter assessed using membrane-coated TEM grids ranges between 14.43 and 26.05 nm (mean value, 19.06 nm), as shown in Supporting Information, Table S2. These values are much smaller than the value, 35.5 nm , observed at $t = 2 \text{ s}$ using a membrane-less TEM grid (Figure 3b), suggesting that the heat-induced deformation is significant even with 1–2 s exposure to electron beam (dilation rate, $\sim 5 \text{ nm/s}$ at $\text{EDR} = 2.3 \text{ e}^- \text{ \AA}^{-2} \text{ s}^{-1}$). Thus, the use of membrane-coated TEM grids is essential for the accurate TEM assessment of tip geometry for sub-10 nm nanopipettes.

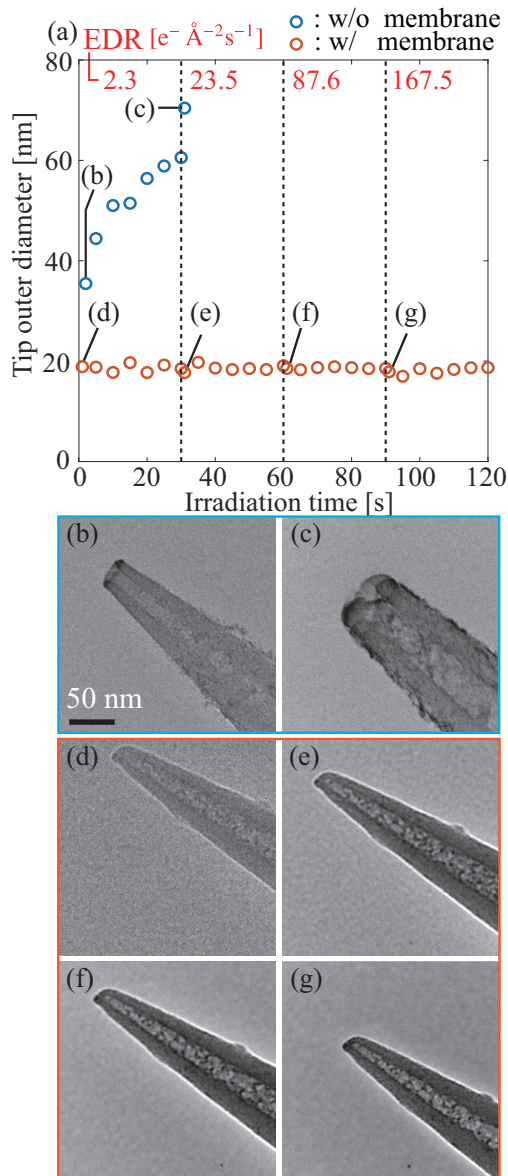


Figure 3. Protective effect of membrane-coating of the TEM grid against deformation of the nanopipette tip in TEM imaging. (a) Tip outer diameter at the tip end as a function of electron irradiation time and electron dose rate, EDR. The red and blue circles represent outer tip diameters measured from time-lapsed TEM images captured using TEM grids with and without the membrane, respectively. The EDR was increased in a stepwise manner from 2.3 to 167.5 $e^{-} \text{ \AA}^{-2} \text{ s}^{-1}$ during the TEM measurements. (b–g) TEM images captured at the time points indicated by letters corresponding to those shown in (a), using TEM grids without the membrane (b,c) and with the membrane (d–g).

*Geometrical Characterization of sub-10 nm Nanopipettes:
TEM Versus $I - V$ Measurements.*

Finally, we discuss how the tip geometry of sub-10-nm nanopipettes is related to the pipette resistance R_p . The

R_p value obtained by electrical measurements is related to the pore diameter d_{pore} and IHC angle θ of the nanopipette, and the solution conductivity κ through the equation

$$d_{pore} = \frac{2}{\kappa R_p} \left(\frac{1}{\pi \tan \theta} + \frac{1}{4} \right). \quad (1)$$

This model [13] assumes a simple conical shape for the tip (i.e., a constant θ). However, the tip regions of sub-10-nm nanopipettes directly captured by TEM revealed deviations from a simple conical shape. Figure 4a depicts the diameter of the inner channel as a function of the distance measured from the tip end (tip distance), extracted from TEM images of eight tip segments with $d_{pore} < 10$ nm (see Supporting Information, sections SI6 and SI7). In all cases the diameter does not increase linearly with the tip distance, that is, the IHC angle θ does not have a single value around the tip, as reported for nanopipettes with larger pore diameters [14]. To check how largely the TEM-assessed geometry of a nanopipette tip affects Equation (1), we used a linearly fitted inner half cone (LF-IHC) angle, defined as the slope obtained by linear fitting of each curve, as shown in Figure 4a for the tip distance from 0 to 200 nm (i.e., approximated IHC angle). For the eight nanopipettes, we compared the values of d_{pore} measured from their TEM images (d_{TEM}) with those estimated using Equation (1), where θ was approximated by the LF-IHC angles (Supporting Information, Table S2). The results are shown in Figure 4b. The two sets of measured values of d_{pore} and d_{TEM} , distributed around ~ 6.4 nm, and their difference were within ± 1.5 nm (SD, $n = 8$); therefore, a relation of $\overline{d_{pore}} - 0.1 \text{ nm} \leq \overline{d_{TEM}} \leq \overline{d_{pore}} + 3.1 \text{ nm}$ holds (95% confidence interval, for $n = 8$), where $\overline{d_{TEM}}$ and $\overline{d_{pore}}$ are the population mean of d_{TEM} and d_{pore} , respectively.

Although the LF-IHC angle gives a good estimate of d_{TEM} , knowing the variation in the IHC angle in the tip region is still important for the numerical analysis of nanofluidic behavior in nanopipettes, since this analysis requires details of the tip geometry. Finite element analysis simulations on the basis of the coupled Poisson, Nernst–Planck, and Navier–Stokes equations have been widely used for the analysis of nanopipettes. This yields spatial profiles of physical quantities (such as potential, ion concentration, flow velocity and pressure) around the nanopipette tip. Such spatial information is difficult to obtain experimentally. Nanofluidic behaviors can be analyzed experimentally for nonlinear $I - V$ relationships, which are generally found in nanofluidic systems with broken symmetry, such as nanopores [21–31] and nanopipettes [32–34]. The combined analysis makes it possible not only to improve the quantitative interpretation of experimental data obtained with nanopipettes but also to extend application of nanopipettes. The TEM method will make significant contributions to

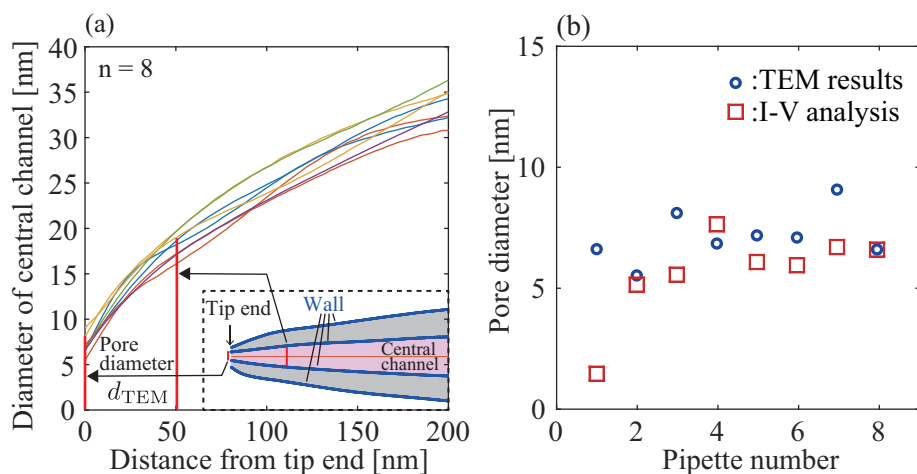


Figure 4. (a) Diameter of the tip central channel of eight nanopipettes measured from their TEM images as a function of distance from the tip end. The inset indicates schematically how the diameter was extracted from a TEM image. The vertical red lines show the diameters corresponding to those shown in the schematic. (b) Comparison of pore diameters measured directly from TEM images of eight nanopipettes (blue circles) to those estimated from $I - V$ measurements for the same nanopipettes (red square).

improving, for example, nano-scale surface charge density (SCD) mapping with SICM [6, 35–39]. The importance of accurate characterization of the tip geometry for SCD measurement was pointed out in previous TEM study [15]. In this application, knowing accurate tip geometries is necessary to quantify the SCD map of the sample because the quantification is sensitive to tip geometries. In fact, quantitative SCD measurements with sub-10 nm spatial resolution is still a challenge [6] because of the difficulty of characterizing the geometrical parameters of sub-10 nm nanopipettes. Besides, our TEM method can provide an opportunity to perform SICM measurements in complicated situations. A recent study [40] revealed a significant contribution of electroosmotic flow and the SCD of the tip to the measured ion current when a large ion concentration gradient exists around a small aperture of the tip. To quantitatively analyze these contributions to the measured SICM data obtained under such conditions [41], information of the detailed tip geometry is indispensable.

The trumpet-like shaped nanopipettes have been frequently observed in electron microscopy measurements [15, 17, 40, 42–47]. However, in this study, we were unable to find appropriate pulling conditions that could produce trumpet-like shaped nanopipettes. This suggests that the trumpet-like shaped nanopipettes are resultant from tip deformation by the electron beam (see Supporting Information, Figures S3 and S5), at least, in TEM measurements of sub-10 nm nanopipettes.

CONCLUSIONS

We have provided the conditions for fabricating sub-10 nm nanopipettes with good reproducibility and procedures for their geometrical characterization by TEM. The TEM imaging following our methods enables quick assessment of tip geometry for many nanopipettes, without deformation of the tip by electron beam-generating heat. Our methods will assist and facilitate the production of smaller nanopipettes and thereby contribute to improving various nanopipette applications.

ASSOCIATED CONTENT

Supporting Information

The Supporting Information is available free of charge at <https://pubs.acs.org/doi/10.1021/acs.analchem.0c02884>. Pulling parameters (SI 1 and Table S1), optimized pulling conditions (SI 2 and Figure S1), photograph of tip segments of sub-10-nm nanopipettes on TEM grid (SI 3, Figure S2), trumpet-like shaped nanopipettes observed under different conditions (SI 4, and Figure S3), dynamics of nanobubbles in sub-10 nm nanopipettes (SI 5 and Figure S4), TEM images of sub-10 nm nanopipettes taken using the membrane-coated TEM grid (SI 6 and Figure S5), geometrical parameters obtained from the TEM images (Table S2), $I - V$ traces of the nanopipettes before characterization by TEM imaging (Figure S6), and procedures for extracting geometrical profiles of nanopipettes (SI 7 and Figure S7), and finite element method simulations and experiments for the estimation of relaxation rate of ion concentration

gradient in the tip (SI8 and Figure S8, Figure S9, and Figure S10) (PDF).

Video files are also provided for procedure of cutting nanopipette (Movie 1).

Procedure for position adjustment of tip segment on TEM grid (Movie 2).

Dynamics of nanobubbles confined in sub-10-nm nanopipette (Movie 3).

AUTHOR INFORMATION

Corresponding Authors

Shinji Watanabe, phone +81(0)76 2344054

Toshio Ando, phone +81(0)76 2645663

ORCID

Kazuki Shigyou:0000-0003-4195-3628

Linhao Sun:0000-0002-4325-7303

Yosuke Kikuchi:0000-0002-2278-821X

Hirotooshi Furusho:0000-0002-6286-5304

Keisuke Miyazawa:0000-0002-5012-8040

Takashi Fukuma:0000-0001-8971-6002

Azuma Taoka:0000-0003-2492-7858

Toshio Ando:0000-0001-8819-154X

Shinji Watanabe:0000-0002-4831-0185

This work was supported by a grant of JST SENTAN (JPMJSN16B4 to S.W.), Grant for Young Scientists from HOKURIKU Bank (to S.W.), JSPS Grant-in-Aid for Young Scientists (B) (JP26790048 to S.W.), JSPS Grant-in-Aid for Young Scientists (A) (JP17H04818 to S.W.), JSPS Grant-in-Aid for Scientific Research on Innovative Areas (JP16H00799 to S.W.) and JSPS Grant-in-Aid for Challenging Exploratory Research (JP18K19018 to S.W.), and JSPS Grant-in-Aid for Scientific Research (S) (JP17H06121 and JP24227005 to T.A.). This work was also supported by a Kanazawa University CHOZEN project and World Premier International Research Center Initiative (WPI), MEXT, Japan.

* tando@staff.kanazawa-u.ac.jp

† wshinji@se.kanazawa-u.ac.jp

‡ Contributed equally to this work

[1] R.-J. Yu, Y.-L. Ying, Y.-X. Hu, R. Gao, and Y.-T. Long, *Analytical chemistry* **89**, 8203 (2017).

- [2] A. P. Ivanov, P. Actis, P. Jönsson, D. Klenerman, Y. Korchev, and J. B. Edel, *ACS Nano* **9**, 3587 (2015).
- [3] J. Y. Sze, S. Kumar, A. P. Ivanov, S.-H. Oh, and J. B. Edel, *Analyst* **140**, 4828 (2015).
- [4] P. Hansma, B. Drake, O. Marti, S. Gould, and C. Prater, *Science* **243**, 641 (1989).
- [5] P. Novak, C. Li, A. I. Shevchuk, R. Stepanyan, M. Caldwell, S. Hughes, T. G. Smart, J. Gorelik, V. P. Ostanin, M. J. Lab, G. W. J. Moss, G. I. Frolenkov, D. Klenerman, and Y. E. Korchev, *Nature methods* **6**, 279 (2009).
- [6] L. H. Klausen, T. Fuhs, and M. Dong, *Nature Communications* **7**, 12447 (2016).
- [7] S. Watanabe and T. Ando, *Applied Physics Letters* **111**, 113106 (2017).
- [8] J. Rheinlaender and T. E. Schäffer, *Analytical chemistry* **87**, 7117 (2015).
- [9] J. Rheinlaender and T. E. Schäffer, *Journal of Applied Physics* **105**, 094905 (2009).
- [10] A. E. Weber and L. A. Baker, *Journal of The Electrochemical Society* **161**, H924 (2014).
- [11] M. A. Edwards, C. G. Williams, A. L. Whitworth, and P. R. Unwin, *Analytical chemistry* **81**, 4482 (2009).
- [12] J. Rheinlaender and T. E. Schäffer, *Analytical chemistry* **89**, 11875 (2017).
- [13] S. Del Linz, E. Willman, M. Caldwell, D. Klenerman, A. Fernández, and G. Moss, *Analytical chemistry* **86**, 2353 (2014).
- [14] E. Tognoni, P. Baschieri, C. Ascoli, M. Pellegrini, and M. Pellegrino, *Micron* **83**, 11 (2016).
- [15] D. Perry, D. Momotenko, R. A. Lazenby, M. Kang, and P. R. Unwin, *Analytical chemistry* **88**, 5523 (2016).
- [16] L. Ying, A. Bruckbauer, A. M. Rothery, Y. E. Korchev, and D. Klenerman, *Analytical Chemistry* **74**, 1380 (2002).
- [17] R. Chen, R. J. Balla, A. Lima, and S. Amemiya, *Analytical chemistry* **89**, 9946 (2017).
- [18] N. Sa and L. A. Baker, *Journal of The Electrochemical Society* **160**, H376 (2013).
- [19] B. J. Polk, A. Stelzenmuller, G. Mijares, W. MacCrehan, and M. Gaitan, *Sensors and Actuators B: Chemical* **114**, 239 (2006).
- [20] L. Sun, K. Shigyou, T. Ando, and S. Watanabe, *Analytical Chemistry* **91**, 14080 (2019).
- [21] Z. S. Siwy, *Advanced Functional Materials* **16**, 735 (2006).
- [22] Z. Siwy and A. Fuliński, *American Journal of Physics* **72**, 567 (2004).
- [23] L.-J. Cheng and L. J. Guo, *Nano Letters* **7**, 3165 (2007).
- [24] E. C. Yusko, R. An, and M. Mayer, *ACS Nano* **4**, 477 (2010).
- [25] L. Cao, W. Guo, Y. Wang, and L. Jiang, *Langmuir* **28**, 2194 (2011).
- [26] Y. Qiu, Z. S. Siwy, and M. Wanunu, *Analytical Chemistry* **91**, 996 (2018).
- [27] Z. Siwy and A. Fuliński, *Physical Review Letters* **89**, 198103 (2002).
- [28] D. Woermann, *Physical Chemistry Chemical Physics* **5**, 1853 (2003).
- [29] J. Cervera, B. Schiedt, and P. Ramirez, *EPL (europhysics letters)* **71**, 35 (2005).
- [30] H. S. White and A. Bund, *Langmuir* **24**, 2212 (2008), pMID: 18225931.
- [31] W.-J. Lan, M. A. Edwards, L. Luo, R. T. Perera, X. Wu, C. R. Martin, and H. S. White, *Accounts of Chemical*

- Research **49**, 2605 (2016).
- [32] C. Wei, A. J. Bard, and S. W. Feldberg, *Analytical Chemistry* **69**, 4627 (1997).
- [33] N. Sa and L. A. Baker, *Journal of the American Chemical Society* **133**, 10398 (2011).
- [34] X. L. Deng, T. Takami, J. W. Son, E. J. Kang, T. Kawai, and B. H. Park, *Scientific reports* **4**, 1 (2014).
- [35] T. Fuhs, L. H. Klausen, S. M. Sønderskov, X. Han, and M. Dong, *Nanoscale* **10**, 4538 (2018).
- [36] D. Perry, B. Paulose Nadappuram, D. Momotenko, P. D. Voyias, A. Page, G. Tripathi, B. G. Frenguelli, and P. R. Unwin, *Journal of the American Chemical Society* **138**, 3152 (2016).
- [37] D. Perry, R. Al Botros, D. Momotenko, S. L. Kinnear, and P. R. Unwin, *ACS nano* **9**, 7266 (2015).
- [38] A. Page, D. Perry, P. Young, D. Mitchell, B. G. Frenguelli, and P. R. Unwin, *Analytical Chemistry* **88**, 10854 (2016).
- [39] K. McKelvey, S. L. Kinnear, D. Perry, D. Momotenko, and P. R. Unwin, *Journal of the American Chemical Society* **136**, 13735 (2014).
- [40] J. Rabinowitz, M. A. Edwards, E. Whittier, K. Jayant, and K. L. Shepard, *The Journal of Physical Chemistry A* **123**, 8285 (2019).
- [41] S. Watanabe, S. Kitazawa, L. Sun, N. Kodera, and T. Ando, *Review of Scientific Instruments* **90**, 123704 (2019).
- [42] L. P. Zweifel, I. Shorubalko, and R. Y. Lim, *ACS Nano* **10**, 1918 (2016).
- [43] M. Holub, M. Adobes-Vidal, A. Frutiger, P. M. Gschwend, S. E. Pratsinis, and D. Momotenko, *ACS Nano* **14**, 7358 (2020), <https://doi.org/10.1021/acsnano.0c02798>.
- [44] N. Sa and L. A. Baker, *Journal of The Electrochemical Society* **160**, H376 (2013).
- [45] R. Hao and B. Zhang, *Analytical Chemistry* **88**, 614 (2016).
- [46] E. M. Yuill, N. Sa, S. J. Ray, G. M. Hieftje, and L. A. Baker, *Analytical Chemistry* **85**, 8498 (2013).
- [47] Z. Zhu, X. Duan, Q. Li, R. Wu, Y. Wang, and B. Li, *Journal of the American Chemical Society* **142**, 4481 (2020).